

#### **PAPER**

# Effects of symmetry and hydrodynamics on the cohesion of groups of swimmers

To cite this article: Mohamed Niged Mabrouk and Daniel Floryan 2025 Bioinspir. Biomim. 20 066005

View the article online for updates and enhancements.

#### You may also like

- Synchronisation through learning for two self-propelled swimmers Guido Novati, Siddhartha Verma, Dmitry Alexeev et al.
- Theoretical framework for twomicroswimmer hydrodynamic interactions Sebastian Ziegler, Thomas Scheel, Maxime Hubert et al.
- Learning to school in dense configurations with multi-agent deep reinforcement learning

Yi Zhu, Jian-Hua Pang, Tong Gao et al.

### **Bioinspiration & Biomimetics**



RECEIVED

15 May 2025

REVISED

16 September 2025

ACCEPTED FOR PUBLICATION 25 September 2025

PUBLISHED

10 October 2025

#### **PAPER**

## Effects of symmetry and hydrodynamics on the cohesion of groups of swimmers

Mohamed Niged Mabrouk Daniel Floryan\*

Department of Mechanical and Aerospace Engineering, University of Houston, Houston, TX 77204, United States of America Author to whom any correspondence should be addressed.

E-mail: dfloryan@uh.edu and mmabrouk@uh.edu

Keywords: swimming, biolocomotion, schooling, fluid dynamics

#### Abstract

When groups of inertial swimmers move together, hydrodynamic interactions play a key role in shaping their collective dynamics, including the cohesion of the group. To explore how hydrodynamic interactions influence group cohesion, we develop a three-dimensional, inviscid, far-field model of a swimmer, neglecting the vortical wake produced by swimmers in order to determine the role that potential flow interactions play on group dynamics. Focusing on symmetric triangular, diamond, and circular group arrangements, we investigate whether passive hydrodynamics alone can promote cohesive behavior, and what role symmetry of the group plays. Under the idealized conditions of our model, we find that far-field interactions alone significantly impact the cohesion of groups of swimmers. This is an important result because, contrary to common belief, it shows that interactions with a vortical wake do not solely determine the cohesion of groups of swimmers. While small symmetric (and even asymmetric) groups can be cohesive, larger groups typically are not, instead breaking apart into smaller, self-organized subgroups that are cohesive. Notably, we discover circular arrangements of swimmers that chase each other around a circle, resembling the milling behavior of natural fish schools; we call this hydrodynamic milling. Hydrodynamic milling is cohesive in the sense that it is a fixed point of a particular Poincaré map, but it is unstable, especially to asymmetric perturbations. Our findings suggest that while passive hydrodynamics alone cannot sustain large-scale cohesion indefinitely, controlling interactions between subgroups, or controlling the behavior of only the periphery of a large group, could potentially enable stable collective behavior with minimal active input.

#### 1. Introduction

In nature, collective behavior is widely observed across animal species [1], where local interactions among individuals give rise to emergent group-level patterns and dynamics. Such behavior is prevalent in groups ranging from insects and fish to birds and mammals, and is critical for enhancing survival and reproductive success [2–5]. Collective coordination enables animals to achieve reciprocal benefits, such as more efficient predator avoidance [6], reduced individual predation risk, and improved foraging and navigation capabilities [7, 8]. Researchers across disciplines like robotics and engineering [9-11] have been drawn to this topic to engineer better swarm

robots that work together in a coordinated manner and match nature's design principles.

Though obvious, it is underappreciated that in order to reap the benefits of collective motion, the collective must remain intact, or cohesive. Maintaining a cohesive group is complicated by the presence of an environment that the individuals must contend with, such as the aerial environments of birds or the aquatic environments of fish. Not only do such environments hold the potential to exert exogenous forcings on the individuals, such as when a bird encounters a gust, or when a group of fish encounters a turbulent flow [12], but they also couple the individuals to each other through fluid-mediated interactions. In this work, we focus on the hydrodynamic

interactions between swimmers—which are expected to play an outsized role in the collective motion of swimmers [13]—specifically on how they affect group cohesion. Our interests lie in schools of swimmers, in which the swimmers display some degree of coordination, as opposed to the broader classification of shoals, in which swimmers are not necessarily coordinated [14].

Weihs' work [15] was the first to link performance improvement in swimmers with hydrodynamic interactions. He argued that a diamond school arrangement is optimal because it creates constructive vortex interactions, allowing trailing fish to gain higher velocity without extra energy expenditure by benefiting from leaders' vortices. Subsequent research has focused on identifying the specific hydrodynamic conditions that enable energy savings through collective swimming formations. Ashraf et al showed that at elevated swimming velocities, fish schools were observed to adopt lateral alignment patterns, with hydrodynamic analysis indicating this configuration reduces energetic costs during sustained high-speed movement [16]. In another study, the authors showed that two fish swimming side by side with a phase difference create a wall effect that reduces energy expenditure [17], building on previous work showing that the wall effect can increase speed, thrust, efficiency, and lower power, though not all at once [18– 22]. Recent work by Heydari et al demonstrated that in larger groups, inline formations unevenly distribute hydrodynamic benefits, with trailing individuals gaining greater energy savings, up to a critical group size [23]. In contrast, side-by-side formations were shown to provide equitable energy savings across all group members while maintaining stable cohesion at any scale. Schooling can evidently provide hydrodynamic benefits when the appropriate group structure is maintained. This motivates our investigation of freely swimming collectives and the dynamics governing their motion, which depend on social interactions, active decision-making, and passive hydrodynamic interactions.

Behavioral models, such as the Vicsek alignment model [24], are widely used to model how individuals interact in a group. They offer a computationally efficient framework for simulating collective behavior in sizable groups. These models and their variants typically incorporate zones of attraction, avoidance, and alignment to describe how individual interactions depend on spatial distribution. The Vicsek model reproduces three stereotypical behaviors observed in fish schools: swarming, milling, and schooling [25, 26]. These behaviors are distinguished by varying degrees of polarization and rotational order, providing insights into the mechanisms underlying collective intelligence in fish groups. Tunstrøm *et al* further demonstrated that both group

size and domain boundaries significantly influence the emergent dynamics of schools [27].

Although schooling dynamics primarily depend on social and sensory mechanisms [25, 28, 29], hydrodynamic effects significantly influence both the interactions and their collective outcomes [30]. Recent studies have combined behavioral models with hydrodynamic interactions to examine collective behavior in fish groups [30–32]. These modeling approaches capture behavioral transitions similar to those observed in the Vicsek model while also considering boundary effects, group size, social interactions between individuals, and flow-mediated interactions. The aforementioned studies focus on twodimensional schools with two-dimensional hydrodynamic interactions. While the precise effects of three-dimensionality on group cohesion and stability are unknown, they undoubtedly differ from the twodimensional case since individual swimmers would not be constrained to planar configurations, and the strength and structure of three-dimensional hydrodynamic interactions differ from two-dimensional interactions.

In previous work, we took a step towards understanding the effects of three-dimensionality by examining the fundamental three-dimensional hydrodynamic interactions between a pair of swimmers [33]. Pairwise interactions serve as a building block for interactions between a larger number of individuals. We found that passive hydrodynamic interactions alone can lead to cohesive pairs of swimmers when their initial configurations are sufficiently well aligned.

In this work, we examine emergent group dynamics arising from three-dimensional hydrodynamic interactions in larger swimmer populations, using the inviscid, far-field model developed in [33]. The reduced-order modeling approach accounts for essential hydrodynamic coupling between swimmers, neglecting the vortical wake produced by swimmers in order to determine the role that potential flow interactions play on group dynamics. By restricting ourselves to potential flow, we may discern the fundamental mechanisms of schooling dynamics. Further details about the choice of the model are provided in the ensuing section. Social and other interactions are not accounted for, allowing us to probe purely hydrodynamic effects and examine to what degree cohesion can emerge from passive hydrodynamic interactions. The study focuses on initially symmetric configurations to determine whether these symmetries persist in the resulting dynamics—a characteristic that can influence group cohesion and promote stable collective motion. Under these idealized conditions, we find that far-field interactions alone significantly impact the cohesion of groups of swimmers. This is an important result because, contrary to common belief,

it shows that interactions with a vortical wake do not solely determine the cohesion of groups of swimmers.

The paper is structured as follows. Section 2 reviews the modeling framework and derives the governing dynamical system. Following that, the free-swimming dynamics of several fundamental configurations of swimmers are explored: triangular configurations in section 3, diamond configurations in section 4, and circular configurations in section 5. A summary and concluding remarks are presented in section 6.

#### 2. Model formulation

Perhaps the most important decision we are faced with is which approach to use to study the group dynamics arising from hydrodynamic interactions. To inform our choice, we turn to real schools of fish. Two characteristics of real schools stand out: they adopt three-dimensional formations [34], and they can be incredibly large, with schools with a million members not uncommon [35]. Although we will restrict ourselves to schools of modest sizes in this work, we ultimately aim to build towards very large schools. Accordingly, we demand that our approach be able to capture three-dimensional interactions for such large schools.

These requirements severely restrict the set of feasible approaches. Experiments cannot fulfill our requirements at cost, nor can high-fidelity simulations. Even an unsteady panel method would quickly become prohibitively expensive for very large schools, as the number of computational flow elements grows linearly with time. Instead, we must turn to a simplified model. For this purpose, in our previous work, we developed a three-dimensional, inviscid, far-field model of a swimmer [33]. The model is inspired by the two-dimensional model developed in [36, 37]. It avoids the cost of other approaches by only considering the inviscid far-field flow induced by a swimmer, ignoring the vortical wake that it produces. More details follow below.

Before proceeding to the technical details of the model, we emphasize that the simplification made by our model is a strategic strength, as it allows one to explore the very interesting space of very large groups of inertia-dominated swimmers. Inevitably, every model system makes tradeoffs between different aspects. We have traded off complexity of the hydrodynamics for access to three-dimensionality and scale, which we argue are fundamental aspects of fish schools. These two fundamental aspects cannot be accessed by other means. Most prior work has sacrificed three-dimensionality and scale for access to higher-complexity hydrodynamics. Of course, real swimmers do produce vortical wakes. We aim not to dismiss the importance of interactions with the wake, but rather to shed light on inviscid far-field effects.

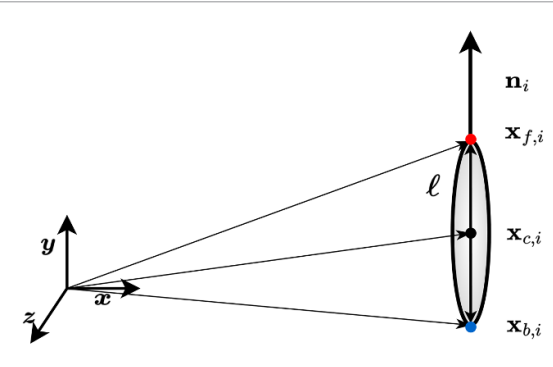


**Figure 1.** Representation of a swimmer modeled as source dipole.

The differing approaches are complementary, as each one brings insights to an aspect of the schooling problem that the other cannot touch.

We proceed by reviewing the essential features of the far-field swimmer model, the details of which can be found in [33]. Each swimmer is modeled as a three-dimensional source-sink pair of equal strength separated by a fixed distance  $\ell$  (see figure 1), producing a dipole flow at large distances. Physically, the source represents the fore of the swimmer, where fluid is expelled in all directions as the swimmer advances, while the sink represents the rear, where fluid is drawn in to fill the void left behind. This model is based on the fact that the potential flow induced by a body of constant volume can be expressed as a multipole expansion in which the leading-order term is a dipole [38, chapter 4.7].

Outside vortical regions and away from boundary layers, the flow is irrotational, justifying the use of a potential flow model. The dipole term in the multipole expansion is a universal feature of swimmers, independent of their specific shape and kinematics—details that are instead encoded in higher-order terms. A comparison of the induced flow to that of a simulated tuna can be found in [33]. Our model provides a computationally tractable way to calculate the flow induced by a swimmer, with broad applicability to inertial swimmers, regardless of their shape characteristics, enabling the study of inviscid mechanisms in groups of swimmers.

In isolation, our model swimmer moves at a speed  $U=\frac{\sigma}{4\pi\,\ell^2}$  along the direction of its body, where  $\sigma\geqslant 0$  is the volumetric flow rate of the source/sink. We call U the self-propelled speed. When more than one swimmer is present, they mutually affect each other's motions through the velocity fields they induce; that is, through their hydrodynamic interactions.

To determine the hydrodynamic interactions, we treat each swimmer as a dumbbell comprising two beads connected by a rigid rod, the beads respectively co-located with the source and sink. Such dumbbell representations are common in the microswimmer literature [39–43]. In this representation, all the

hydrodynamic forces experienced by the swimmer are concentrated on the beads, and the rigid rod serves to keep the length of the dumbbell fixed. Using the results developed in [44] for the force on a sphere in an unsteady inviscid flow, and assuming the bead is neutrally buoyant—a reasonable assumption in the context of swimming—it can be shown that the bead moves as a material point [33]. Thus, for each swimmer, we take the velocity of the source (sink) to be equal to the sum of the self-propelled velocity and the velocity induced by the sources and sinks of all other swimmers. A small modification must be made to the velocity of each bead in order to ensure that the length of the dumbbell is constant in time, which is discussed in the ensuing text.

In this work, we consider a system of N identical swimmers. We denote by  $\mathbf{x}_{f,i}$  and  $\mathbf{x}_{b,i}$  the position vectors of the source and sink of the ith swimmer, respectively (figure 1). Let  $\mathbf{x}_{c,i}$  be the center position and  $\mathbf{n}_i$  the orientation vector pointing from the sink to the source. We can express  $\mathbf{x}_{f,i}$  and  $\mathbf{x}_{b,i}$  in terms of of  $\mathbf{x}_{c,i}$ ,  $\mathbf{n}_i$ , and  $\ell$ :

$$\mathbf{x}_{f,i} = \mathbf{x}_{c,i} + \frac{1}{2}\ell\mathbf{n}_i, \tag{1a}$$

$$\mathbf{x}_{b,i} = \mathbf{x}_{c,i} - \frac{1}{2}\ell\mathbf{n}_i. \tag{1b}$$

Each swimmer is thus described by six variables: three for the center coordinates and three for the orientation vector. (If desired, the orientation can instead be described by two angular variables).

The translational and rotational dynamics of each swimmer are given by

$$\frac{d\mathbf{x}_{c,i}}{dt} = \frac{1}{2} \left( \mathbf{v}_{f,i} + \mathbf{v}_{b,i} \right), \qquad (2)$$

$$\frac{d\mathbf{n}_{i}}{dt} = \frac{1}{\ell} \left( \mathbf{v}_{f,i} - \mathbf{v}_{b,i} + 2\lambda_{i} \mathbf{n}_{i} \right)$$

$$= \frac{1}{\ell} \left\{ \mathbf{v}_{f,i} - \mathbf{v}_{b,i} - \left[ \left( \mathbf{v}_{f,i} - \mathbf{v}_{b,i} \right) \cdot \mathbf{n}_{i} \right] \mathbf{n}_{i} \right\}. \quad (3)$$

Above,  $\mathbf{v}_{f,i}$  and  $\mathbf{v}_{b,i}$  respectively correspond to the unconstrained velocities of the source and sink of the *i*th swimmer due to the self-propelled velocity and the interactions with other swimmers, given by

$$\mathbf{v}_{f,i} = U\mathbf{n}_{i} + \frac{\sigma}{4\pi} \sum_{\substack{j=1\\j\neq i}}^{N} \left( \frac{\mathbf{x}_{f,i} - \mathbf{x}_{f,j}}{\left\| \mathbf{x}_{f,i} - \mathbf{x}_{f,j} \right\|^{3}} - \frac{\mathbf{x}_{f,i} - \mathbf{x}_{b,j}}{\left\| \mathbf{x}_{f,i} - \mathbf{x}_{b,j} \right\|^{3}} \right),$$

$$(4a)$$

$$\mathbf{v}_{b,i} = U\mathbf{n}_i + \frac{\sigma}{4\pi} \sum_{\substack{j=1\\j\neq i}}^{N} \left( \frac{\mathbf{x}_{b,i} - \mathbf{x}_{f,j}}{\left\| \mathbf{x}_{b,i} - \mathbf{x}_{f,j} \right\|^3} - \frac{\mathbf{x}_{b,i} - \mathbf{x}_{b,j}}{\left\| \mathbf{x}_{b,i} - \mathbf{x}_{b,j} \right\|^3} \right). \tag{4b}$$

The Lagrange multiplier  $\lambda_i$  in equation (3) ensures the constraint  $\frac{d\ell}{dt} = 0$  is satisfied for all swimmers, maintaining the constant distance between the source and sink during motion. It originates from a force that

acts on the source and the sink to either push them toward each other or pull them apart, as needed. This force does not produce any net translation or rotation of the *i*th swimmer, nor does it directly affect the hydrodynamic interactions between swimmers. For more details, see [33].

We concatenate the position and orientation vectors of all swimmers into a single state vector  $\mathbf{X}$  of dimension 6N. The state of the system is evolved forward in time numerically using the fourth-order Runge–Kutta method. At each step, we re-normalize the orientation vectors  $\mathbf{n}_i$  to ensure they have unit length during the simulation. For all the results shown in this work, lengths have been normalized by  $\ell$ , velocities by U, and time by  $\ell/U$ .

#### 3. Triangular configurations

We start by investigating the simplest groups with N > 2: triangular configurations of swimmers. Five parameters are required to describe the state of our model swimmer: three for its center position and two for its orientation. It therefore seems that 15 parameters are required to describe the state of a trio. The required number of parameters can be reduced to nine by leveraging the continuous translational and rotational symmetries of the system. Even with this reduction, it is infeasible to characterize the dynamics of a trio in such a large parameter space.

We therefore focus on a reduced set of configurations that are of the leader-follower type, as sketched in figure 2. Without loss of generality, we fix one swimmer at the origin and orient it in the positive *y*-direction. By making the other two swimmers coplanar with the first and imposing mirror symmetry about the *y*-axis, the configuration of the trio simplifies to being described by two separation parameters,  $\Delta x$  and  $\Delta y$ , and a relative angle between the symmetric pair,  $\Delta \theta$ . Due to the mirror symmetry, we need only consider initial configurations with  $\Delta x > 0$ . When  $\Delta y > 0$ , the trio is arranged as one leader and two followers (which we will also refer to as trailing swimmers). Conversely,  $\Delta y < 0$  gives two leaders and one follower.

Owing to translational symmetry, only the separations  $\Delta x$  and  $\Delta y$  between the swimmers, not the absolute positions, affect the dynamics. Rotational symmetry further implies that only the relative angle  $\Delta \theta$  between the symmetric pair influences the system, as the central swimmer experiences no net rotation or translation in the x-direction. The symmetric pair can either enhance or oppose the central swimmer's motion along its axis, while their mirrored hydrodynamic fields preclude lateral motion of the central swimmer.

Several distinct dynamical regimes emerge, depending on the swimmers' initial configuration. The simplest case occurs when  $|\Delta y| \to \infty$ , where the

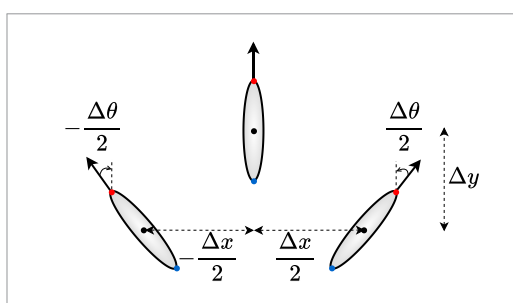


**Figure 2.** Configuration of three swimmers with mirror symmetry about the *y*-axis. One swimmer is fixed at the origin, while the other two swimmers are positioned symmetrically.

central swimmer moves at its self-propelled speed and the rest of the system effectively reduces to a two-swimmer interaction. In this limit, the two swimmers either end up in deadlock (for  $\Delta\theta = -\pi$ ), collide (for small  $\Delta x$ ), or diverge (for all other parameter values); see [33] for details. The collision scenario is non-physical in our model since a far-field model does not accurately model hydrodynamic interactions when the swimmers are too close.

For finite  $\Delta y$ , it is useful to think of the symmetric pair as being perturbed by the presence of the central swimmer. All three swimmers now interact, and new dynamical states emerge. We first consider the case where  $\Delta y > 0$ , corresponding to one leader and two trailing swimmers, before continuing to the case where  $\Delta y < 0$ , corresponding to two leaders and one trailing swimmer.

#### 3.1. One leader, two trailing swimmers

For initial configurations where all three swimmers are aligned ( $\Delta\theta=0$ ), the phase diagram in figure 3 summarizes the dynamical states that result. The swimmers either collide, diverge, or oscillate as a cohesive group. We distinguish four regions in the phase diagram.

Region I consists of tall and narrow configurations of the trio for which the swimmers eventually diverge. The velocity field induced by the leader pulls the trailing swimmers forward towards it, closer towards each other, and tends to rotate them towards each other. The velocity field induced by the trailing swimmers has an opposing effect: it pushes the leader further away, slows down the trailing swimmers, and rotates them away from each other. Because of the tall and narrow configuration, the trailing swimmers are more strongly affected by each other's hydrodynamic fields than the leader's, leading them to rotate away from each other. Furthermore, while the trailing swimmers are pulled forward by the lone leader, the leader is pushed forward by two trailing swimmers, the net effect being that the leader separates from the trailing swimmers.

A representative case is shown in figure 4(a). The vertical separation  $\Delta y$  increases monotonically while the lateral separation  $\Delta x$  first decreases by a very small amount, reaches a minimum, and then increases. This is accompanied by the two trailing swimmers rapidly rotating away from each other, overshooting their steady-state orientations, before gradually rotating back towards each other and approaching their steady-state orientations, where they face away from each other. (In order to better illustrate the early dynamics, the configurations shown in figure 4(a) occur before the overshoot. The dynamics up to and after the overshoot would be difficult to visually distinguish since the overshoot is weak). As they rotate, their self-propelled velocity acquires a lateral component, driving the swimmers outward. As they further separate, the hydrodynamic interactions weaken relative to their self-propelled velocities. Once sufficiently separated, the swimmers are essentially independent of each other, moving forward at their self-propelled speeds, askew, continuing to separate from each other.

Short and wide configurations also lead the swimmers to diverge from each other, captured by region II in the phase diagram. For such configurations, all the hydrodynamic interactions tend to rotate the trailing swimmers away from each other. The velocity field induced by the leader pulls the trailing swimmers closer to each other. In contrast to the tall and narrow configurations of region I, now the trailing swimmers pull the leader towards them, while the leader pushes the trailing swimmers away from it. Once again, the combined might of the trailing swimmers is stronger, causing the separation in the y-direction to initially decrease. A representative case is shown in figure 4(b). The lateral and vertical separation of the swimmers initially decreases while the trailing swimmers rotate outward. As they rotate, their selfpropelled velocity acquires a lateral component. This lateral component dominates the induced velocities from the other swimmers once they have rotated sufficiently, causing the lateral separation  $\Delta x$  to begin to increase. As they continue to separate laterally, the hydrodynamic interactions weaken, and soon the self-propelled velocity dominates the dynamics. At this point, the swimmers move askew from each other along nearly straight lines at their self-propelled speeds, separating vertically and laterally at steady

Oscillatory dynamics emerge in two adjacent regions (regions III and IV) of the phase diagram. Representative cases are shown in figures 4(c) and (d), respectively. In both regions,  $\Delta y$  increases monotonically while  $\Delta x$  exhibits oscillatory behavior on top of a net increase. Similarly, the relative angle  $\Delta \theta$  oscillates between positive and negative values. Regions III and IV are distinguished by their initial rotational dynamics, with the trailing swimmers

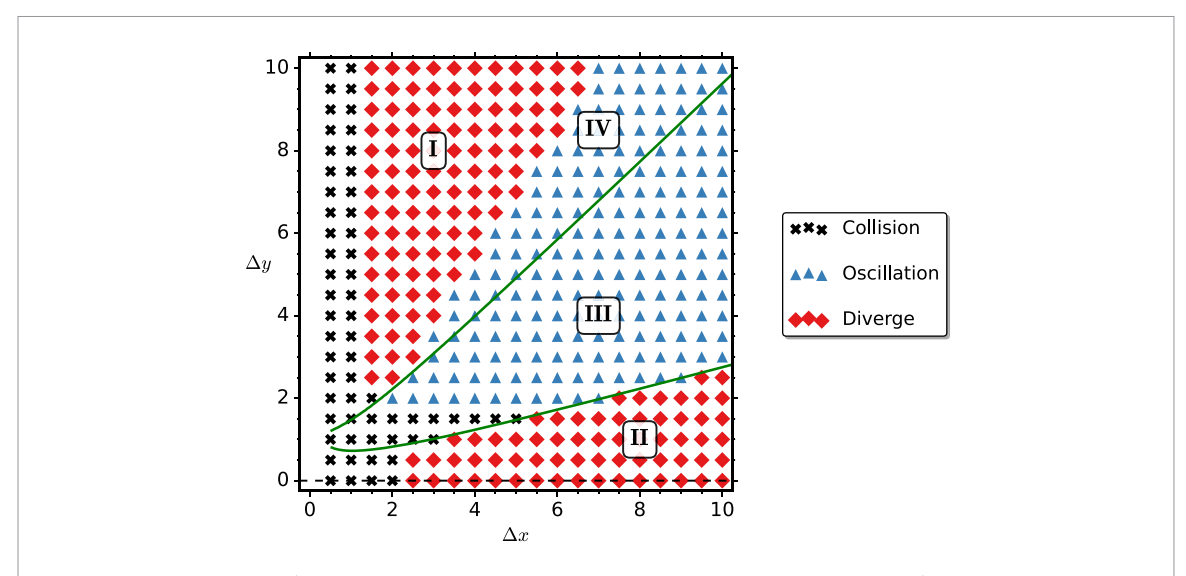


**Figure 3.** Phase diagram for  $\Delta\theta=0$  for three swimmers, with one leader and two trailing swimmers ( $\Delta y>0$ ). The green curves correspond to states of the system satisfying  $\frac{d\mathbf{n}}{dt}\cdot\mathbf{e}_1=0$ , where  $\mathbf{e}_1$  is the unit vector in the positive *x*-direction.

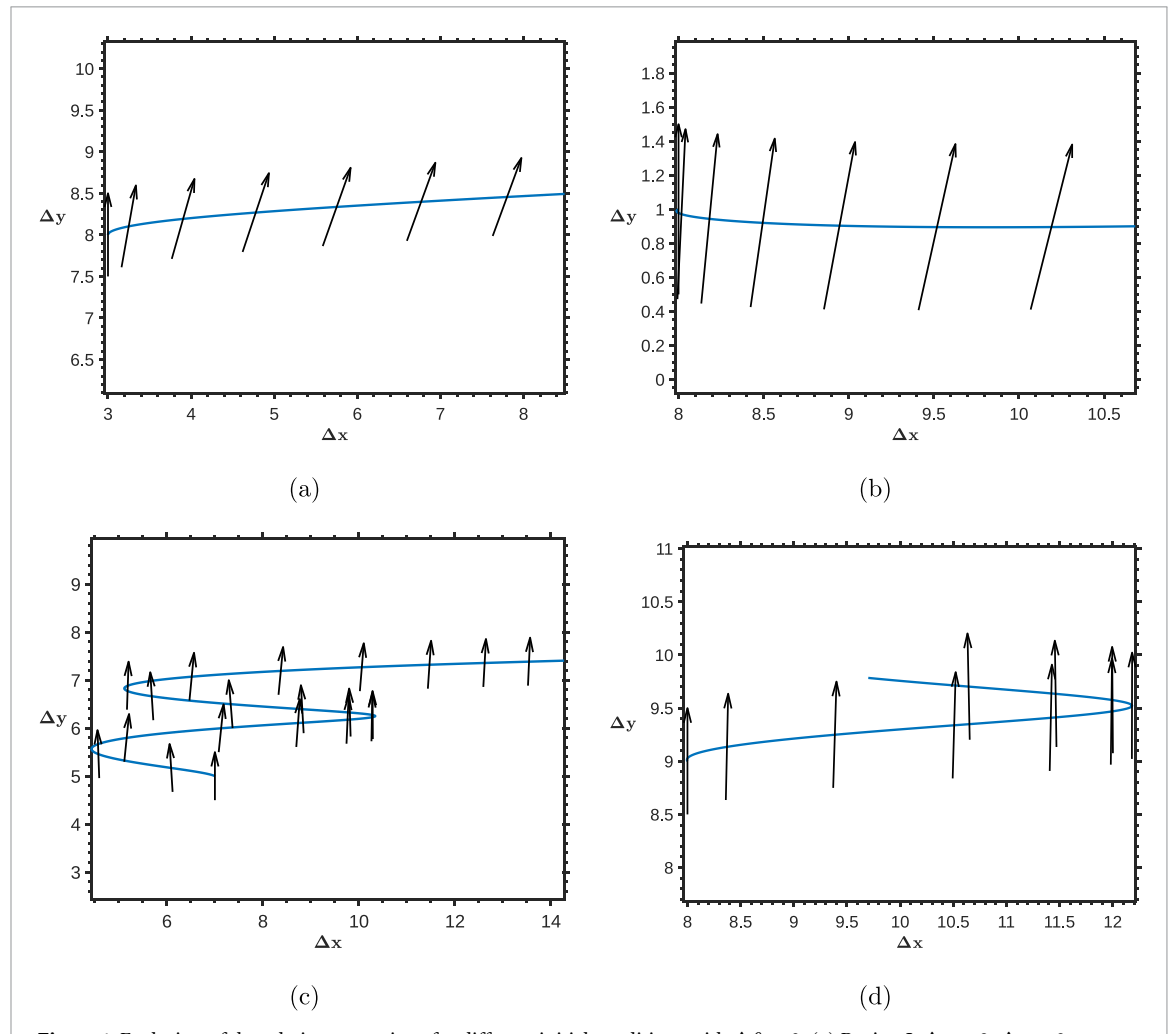


**Figure 4.** Evolution of the relative separations for different initial conditions with  $\Delta\theta=0$ . (a) Region I:  $\Delta x=3$ ,  $\Delta y=8$ . (b) Region II:  $\Delta x=8$ ,  $\Delta y=1$ . (c) Region III:  $\Delta x=7$ ,  $\Delta y=5$ . (d) Region IV:  $\Delta x=8$ ,  $\Delta y=9$ . The arrows indicate the vector  $(\sin \Delta\theta, \cos \Delta\theta)$ , i.e. they are rotated clockwise from the vertical by  $\Delta\theta$ . N.B.: the plots illustrate the trajectory of the system in the symmetry-reduced space, not the paths taken by the swimmers.

initially rotating inward in region III, whereas they initially rotate outward in region IV. The boundary between the two regions is thus given by the locus of initial configurations for which  $\frac{d\mathbf{n}}{dt} \cdot \mathbf{e}_1 = 0$ , where  $\mathbf{e}_1$  is the unit vector in the positive x-direction. This boundary is drawn as a solid green curve in figure 3. The two regions are highly intertwined, however. In figures 4(c) and (d), one can see that  $\Delta\theta$  becomes zero at the extremes of the oscillations, and  $\frac{d}{dt}\Delta\theta$  changes sign from one extreme to the next. This implies that swimmers whose initial configuration lies in region III move to a configuration lying in region IV, and vice versa. As a result, the swimmers oscillate between the two regions. Physically, when the trailing swimmers are close (i.e. in region IV), they influence each other more strongly than the leader does. The trailing swimmers always rotate each other outward in this region, causing their self-propelled velocities to acquire a lateral component that moves the trailing swimmers apart. Once the trailing swimmers are sufficiently far apart, the influence of the leader becomes relatively stronger. The leader has a tendency to rotate the trailing swimmers inward, which overcomes the outward rotation that the trailing swimmers induce on each other. The trailing swimmers thus rotate inward, reaching region III, and continue rotating to the point where their self-propelled velocities acquire a lateral component that moves them towards each other. The process repeats cyclically.

The swimmers do not oscillate forever, eventually diverging. The number of oscillations that occur before divergence depends on the initial separation of the swimmers. We have observed anywhere from one oscillation to over 50 oscillations complete before the swimmers diverge. The time between oscillations increases rapidly, in some cases increasing exponentially with the number of oscillations. Since the separation between the leader and the trailing swimmers increases with each cycle, the hydrodynamic influence of the leader on the trailing swimmers decreases from one cycle to the next. As a result, the ability of the leader to rotate the trailing swimmers inward weakens from one cycle to the next. Once the separation has reached a critical value, the leader is unable to rotate the trailing swimmers inward, and they diverge, traveling away at their self-propelled speeds. There is no simple relation for the critical separation since it depends on the maximal relative angle between the trailing swimmers during the oscillations.

In addition to the boundary separating regions III and IV, there is another locus of configurations for which  $\frac{d\mathbf{n}}{dt} \cdot \mathbf{e}_1 = 0$  in figure 3. This forms the boundary between the configurations that lead to divergence in region II and those that lead to oscillatory behavior in region III. Such a simple criterion separating the oscillatory configurations of region IV from the diverging configurations of region I does not exist. In both regions I and IV, the trailing swimmers initially

rotate outward and then inward. In region I, however, the trailing swimmers attain a larger relative angle  $\Delta\theta$ , causing them to laterally separate at a faster rate, which causes the hydrodynamic influence of the leader on the trailing swimmers to decay at a faster rate. The leader does not rotate the trailing swimmers inward sufficiently fast, and they diverge from each other. This is analogous to the escape velocity required for an object to escape the gravitational pull of a planet.

Since the configurations in regions I and II lead to divergence, such trios are not cohesive. While the configurations in regions III and IV lead to hydrodynamic interactions that lock the trio into a dynamically coupled state, their vertical and lateral separations increase on net, and the swimmers eventually diverge. We therefore consider regions III and IV to give rise to semi- (or finite-time) cohesion. For  $\Delta\theta\neq 0$ , the region of phase space leading to divergence increases in size.

#### 3.2. Two leaders, one trailing swimmer

The phase diagram for a trio with two leaders and one trailing swimmer is shown in figure 5. Qualitatively, it is very similar to the phase diagram for one leader with two trailing swimmers: when the swimmers are too close, they collide with each other; and when the aspect ratio  $\Delta y/\Delta x$  of the trio is large or small, the swimmers diverge from each other.

The primary difference between the phase diagrams is the emergence of a stable relative equilibrium when there are two leaders and one trailing swimmer. No stable state exists for the case of one leader and two trailing swimmers. The purple circles in figure 5 show the initial configurations of the trio (with  $\Delta\theta = 0$ ) that converge to the relative equilibrium. The relative equilibrium itself and its induced velocity field are shown in figure 6. The swimmers are configured as an isosceles triangle, with the two leaders facing slightly inward. The group maintains its configuration while moving forward at a speed equal to 0.934*U*, slower than the self-propelled speed of an isolated swimmer. A similar result was demonstrated by Tchieu et al in [36], where a trio of counter-rotating point-vortex pairs evolved toward a stable equilibrium in which the pairs face each other and form an equilateral triangle. Due to their configuration, the vortex pairs do not move. In our case, the configuration is different, and the group has a non-zero speed.

A key feature of the relative equilibrium is its robustness to perturbations in  $\Delta x$ ,  $\Delta y$ , and  $\Delta \theta$ . The basin of attraction of the relative equilibrium is shown in figure 7, where configurations inside the curves converge to the relative equilibrium. The central swimmer, now trailing the symmetric pair, induces the same rotational dynamics on the symmetric pair as when it was the leader. The translational dynamics that it induces, however, differ. Rather than drawing

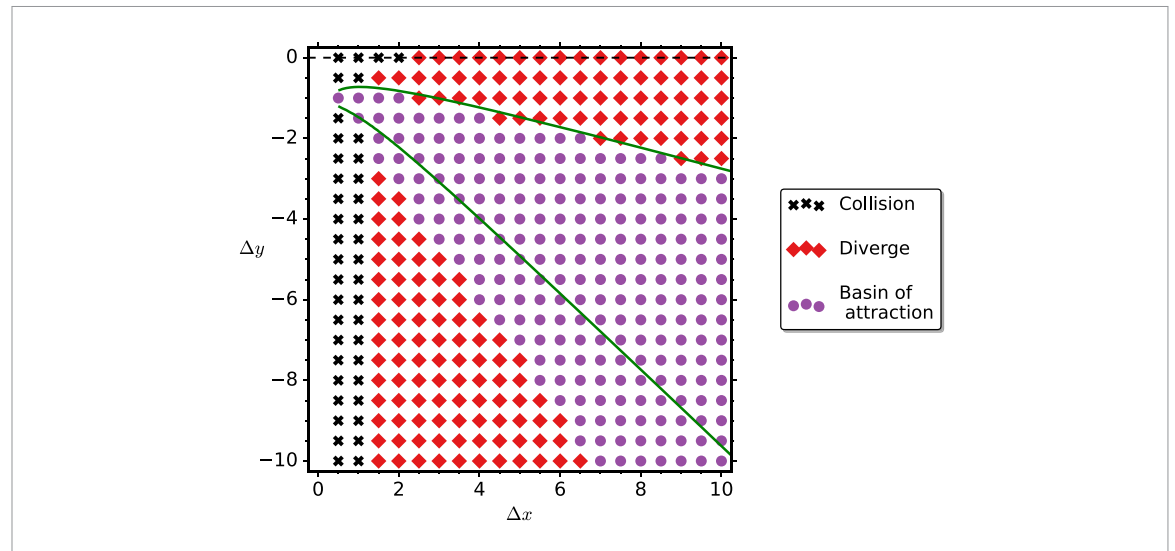
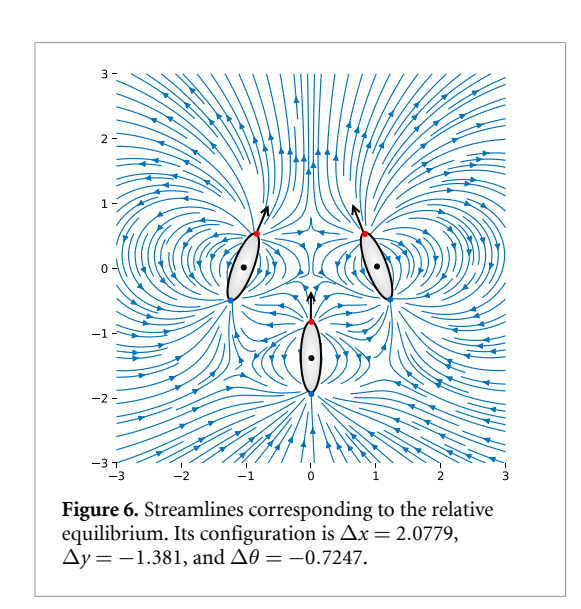


**Figure 5.** Phase diagram for  $\Delta \theta = 0$  for three swimmers, with two leaders and one trailing swimmer ( $\Delta y < 0$ ). The green curves correspond to states of the system satisfying  $\frac{d\mathbf{n}}{dt} \cdot \mathbf{e}_1 = 0$ , where  $\mathbf{e}_1$  is the unit vector in the positive *x*-direction.



the pair together, the central swimmer pushes them apart when it is in the trailing position. This difference leads to the emergence of the relative equilibrium. In the equilibrium configuration, the outward rotation that the leaders induce on each other is balanced by the inward rotation induced by the trailing swimmer, and the lateral components of the self-propelled velocities of the leaders are balanced by the laterally outward push induced by the trailing swimmer.

#### 4. Diamond configurations

By composing triangular configurations of swimmers, one can create a diamond configuration. In his seminal work, Weihs argued that by arranging themselves into a diamond formation, swimmers stand to expend less energy than in isolation [15]. Since

then, diamond formations have been among the most studied. Here, we characterize the cohesion of such a formation.

The stability of diamond lattices of swimmers was previously studied in [11], where it was found that diamond formations are not passively stable. An important distinction between that work and the present work is how the swimmers are modeled. While both utilize a far-field model for the swimmers, Gazzola et al used the model of [36], wherein a swimmer is modeled as a planar pair of point vortices separated by a fixed distance. This produces the same farfield flow as a two-dimensional version of our model, but leads to qualitatively different rotational dynamics due to how the velocity gradient is sampled by the swimmer. As argued in [33], the vortex-pair model is appropriate for short and wide swimmers, whereas the model used in the present work is appropriate for the more commonly encountered long and narrow swimmers. This key difference may lead to a change in the stability/cohesion of a diamond arrangement of swimmers, as suggested by the results in section 3.2.

The diamond arrangement is shown in figure 8, characterized by the spacings  $\Delta x$  and  $\Delta y$ . We examine three representative cases with group sizes N=7, 13, and 27 swimmers, with fixed spacings of  $\Delta x=\Delta y=16$ , whose trajectories are shown in figure 9. All configurations shown have mirror symmetry.

Several dynamical features emerge. Most obviously, the central swimmers experience neither rotation nor transverse translation. This is a consequence of being along the axis of symmetry. The other swimmers are symmetric about this axis. In fact, the central axis behaves as an impermeable wall since the mirror symmetry is equivalent to using the method of images for potential flows. Consequently, swimmers do not cross the central axis. Surprisingly, the

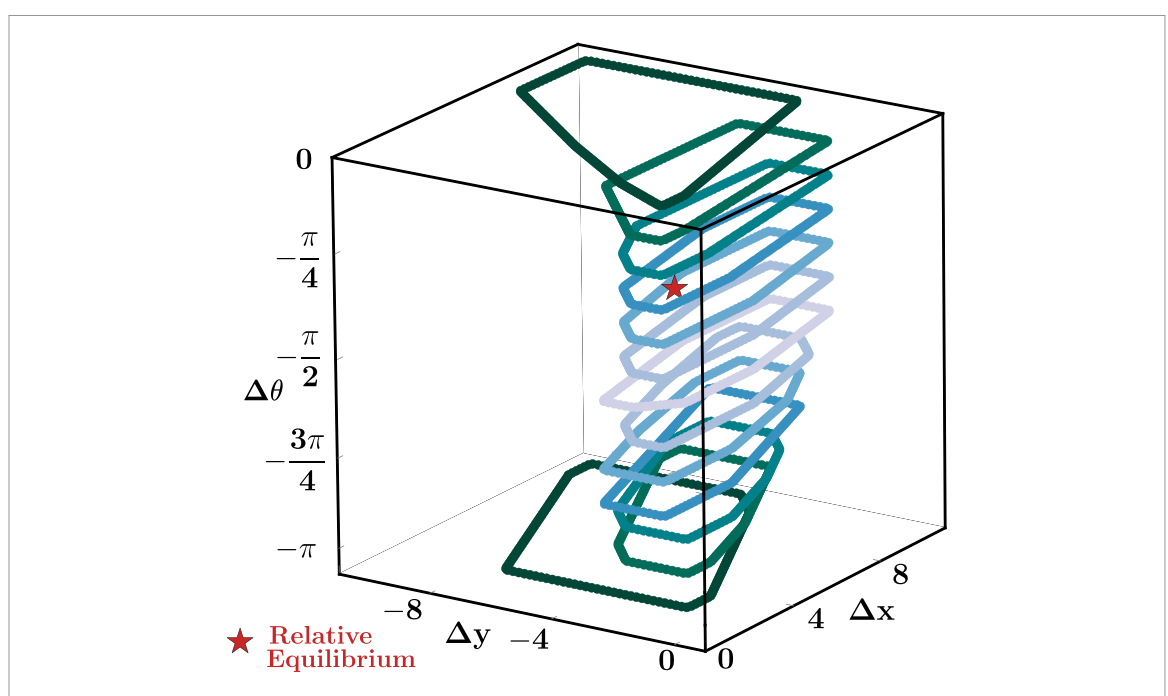


**Figure 7.** Basin of attraction for the relative equilibrium in figure 6, for  $\Delta x$ ,  $\Delta y \le 10$ . Curves are plotted in steps of  $\pi/12$  in  $\Delta\theta$ .

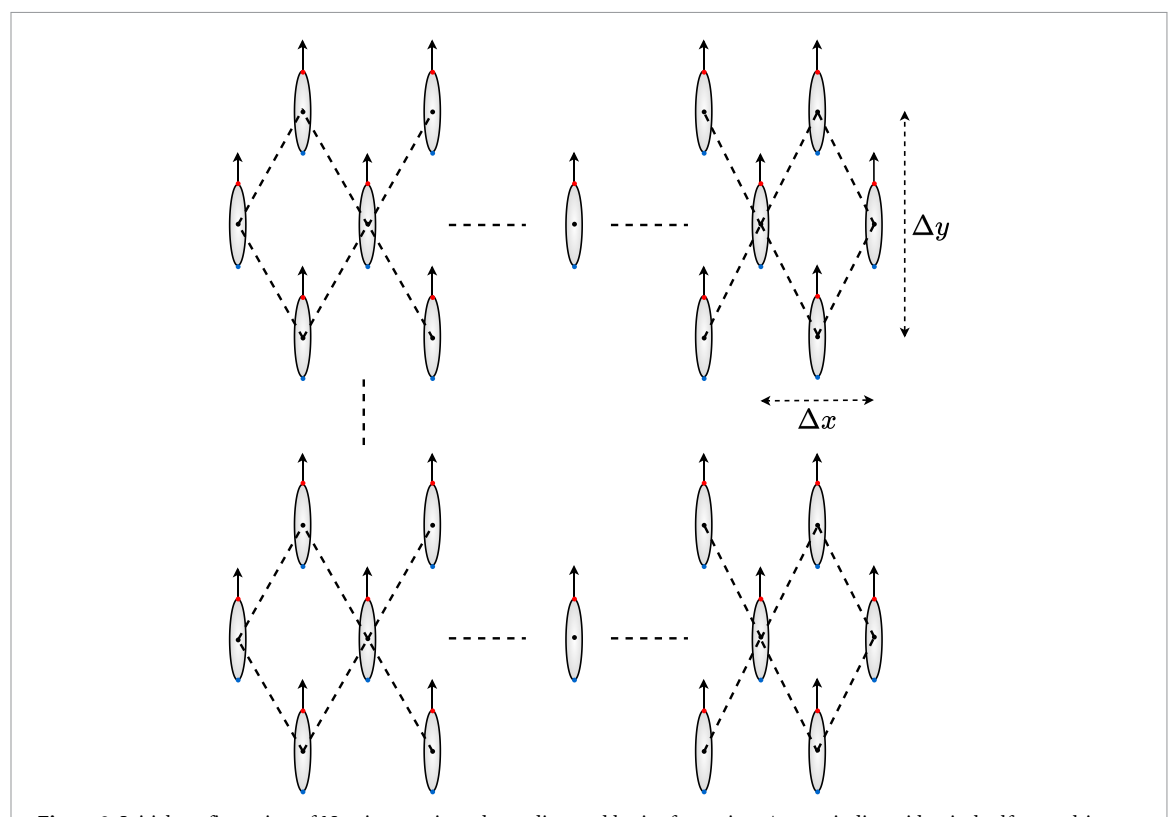


**Figure 8.** Initial configuration of N swimmers in a planar diamond lattice formation. Arrows indicate identical self-propulsion directions, with uniform lattice spacings  $\Delta x$  and  $\Delta y$  throughout the school.

symmetry eventually breaks in figure 9(c); we will elaborate on this observation later.

In the smallest group, the peripheral swimmers separate into subgroups of three swimmers that oscillate in a braided pattern, which often happens to pairs of swimmers [33]. The braided trios slowly

diverge from each other, and this divergence continues beyond what is plotted, though each subgroup seems to maintain its structure. Although the entire group remains cohesive for only a finite time, the emergent subgroups remain cohesive for much longer.

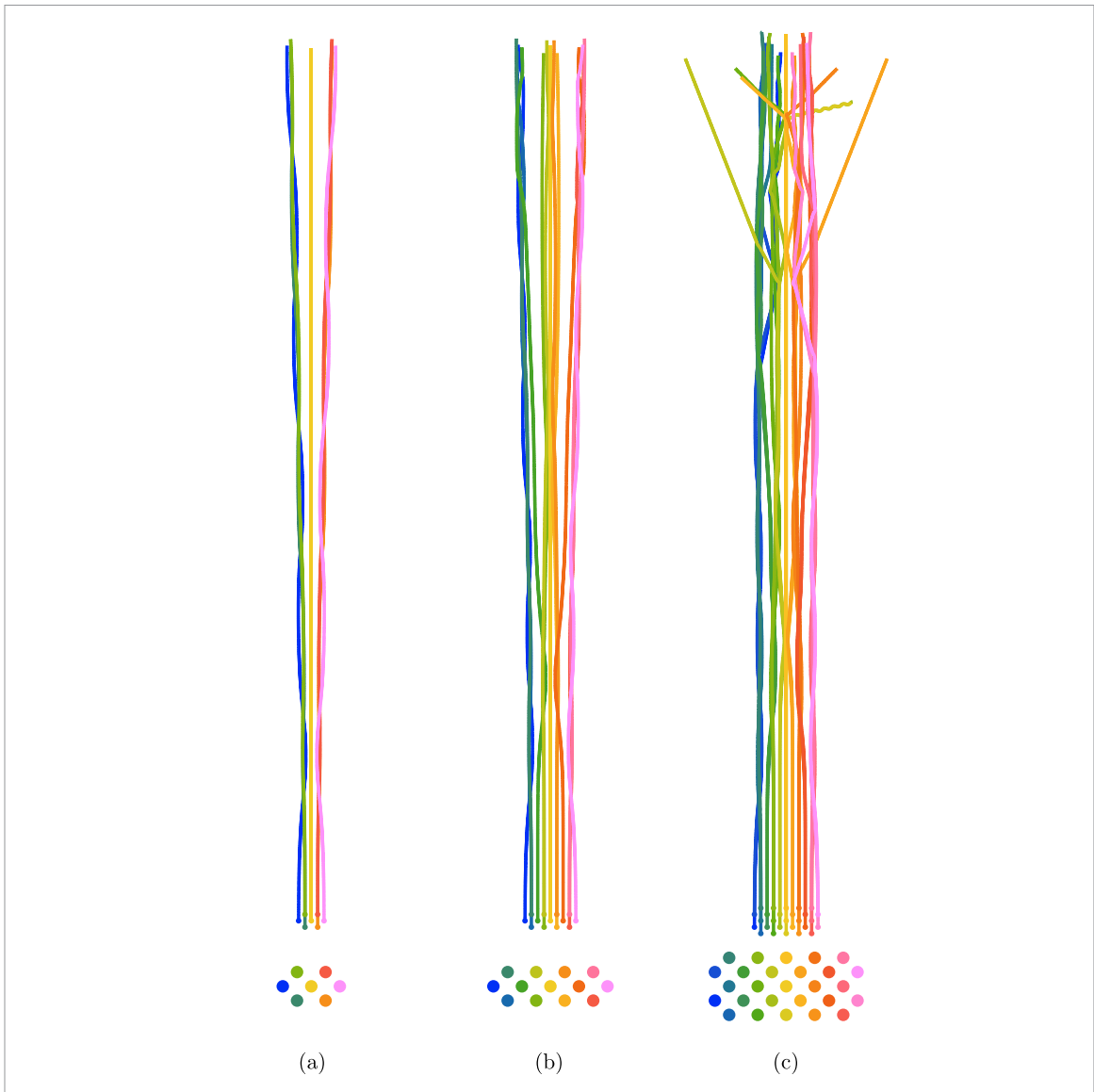


**Figure 9.** Planar trajectories of *N* swimmers for different initial conditions. (a) N = 7,  $\Delta x = 16$ ,  $\Delta y = 16$ . (b) N = 13,  $\Delta x = 16$ ,  $\Delta y = 16$ . (c) N = 27,  $\Delta x = 16$ ,  $\Delta y = 16$ . The patterns on the bottom show the initial arrangements. The trajectories are shown at time t = 1000.

The larger diamond formations initially display similar behavior, though in stages. In figure 9(b), the outermost swimmers (blue and pink) are the first to form braided trios and move slightly inward. Later, the next layer of swimmers (green and orange) organize into another set of braided trios that move inward. The behavior is similar for the largest group of swimmers in figure 9(c), with the outermost swimmers (blue and pink) forming braided quintets, followed by the next layer (green and orange) forming another set of braided quintets, and finally followed by the last layer (light green and light orange) forming braided pairs, all of which move inward. The core of the group is able to sustain nearly straight motion for a longer time than the periphery for the same reason that the central swimmers maintain straight motion: they experience opposing hydrodynamic interactions with swimmers on either side. For example, consider the light green swimmers just left of center in figure 9(c).

Only the five outermost pink swimmers on the right can cause the light green swimmers to translate laterally or rotate since every other swimmer has an opposite with respect to the light green swimmers that nullifies any induced lateral translation or rotation. Swimmers closer to the periphery experience less such cancellation of hydrodynamic interactions, which is why they veer off straight paths earlier. The blue swimmers on the left, for example, have no leftward neighbors that can oppose the lateral translation and rotation induced by their rightward neighbors, leading the blue swimmers to veer off first.

Once all braided subgroups have formed from the outside in, they begin to diverge from the inside out. At this point, the dynamics become quite complex, and interactions between subgroups emerge. We observe that swimmers sometimes switch the subgroup they belong to, that subgroups exchange

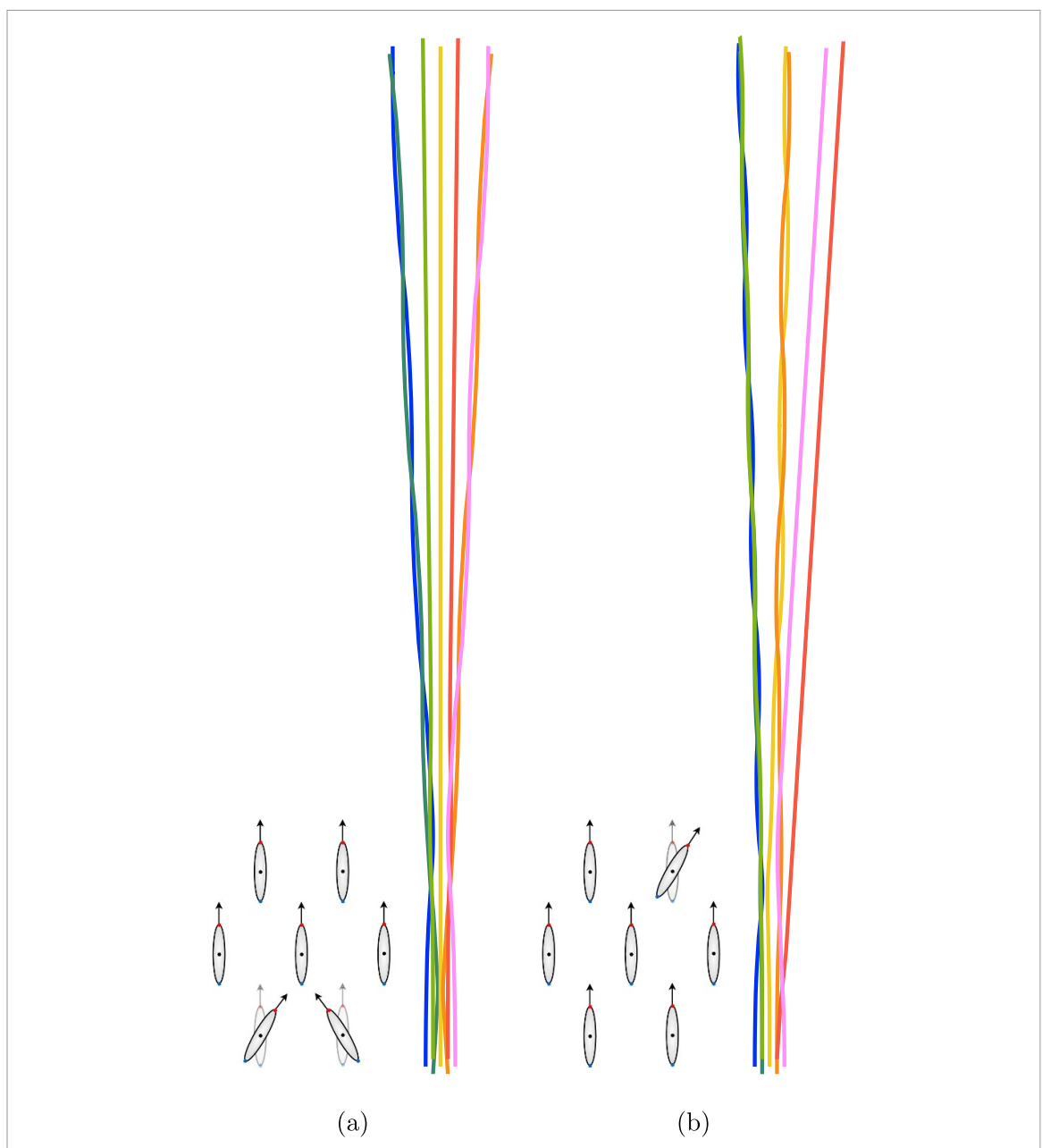


**Figure 10.** Perturbed configurations and corresponding trajectories for N=7. (a) Symmetric rotation of two swimmers. (b) Asymmetric rotation of one swimmer. The perturbed swimmers are initially rotated  $\pi/48$  from the vertical. The trajectories are shown at time t=1000.

positions, and individual swimmers are ejected from the group. Overall, the group begins to progressively lose cohesion, though not in a catastrophic manner. The eventual loss of cohesion results from a chain of events that starts from the periphery of the group. This suggests that the inner core of a group is passively cohesive, and the cohesion of the overall group can be maintained by actively adjusting or controlling the behavior of the swimmers on the periphery while allowing the inner core of swimmers to passively evolve.

As we remarked earlier, the largest group in figure 9(c) loses mirror symmetry. This also happens to the smaller group in figure 9(a) a bit beyond what has been plotted. Round-off error in

our simulations breaks the mirror symmetry; once broken, the dynamics of the system evolve the group further away from a symmetric configuration, which suggests that certain symmetries are not robust to perturbations.

To qualitatively assess the robustness of the diamond arrangement, we consider two types of perturbations for the case N=7. The first is a symmetric perturbation, in which two swimmers are rotated while preserving mirror symmetry. The second is an asymmetric perturbation, where only one swimmer is rotated, thereby breaking the mirror symmetry. The perturbations and resulting trajectories are shown in figure 10, and should be compared to the unperturbed trajectory in figure 9(a).

For the symmetrically perturbed case, two swimmers are initially rotated towards each other by  $\pi/48$ , maintaining the overall mirror symmetry of the arrangement, as illustrated in figure 10(a). The swimmers spread out at a faster rate than in the unperturbed case. Further differences arise in the structure of the subgroups, with the peripheral swimmers forming braided pairs instead of trios. Compared to the unperturbed case, one could say that the overall cohesion is somewhat lower, but the dynamics are qualitatively quite similar.

For the asymmetrically perturbed case, one swimmer is initially rotated outward by  $\pi/48$ , breaking the mirror symmetry of the arrangement, as shown in figure 10(b). The swimmers spread out at a faster rate than in the unperturbed case, but at approximately the same rate as in the symmetrically perturbed case. Subgroups emerge as before; now, the leftmost braided trio from the unperturbed case arises again, and a new central braided pair emerges (though upon closer inspection, the orange swimmer is initially entangled with the red and pink swimmers before finally pairing with the central yellow swimmer).

Overall, loss of symmetry seems to somewhat lower the cohesion of the group. What is robust to perturbations, however, is the emergence of subgroups that seem to remain cohesive throughout their lifetimes. The emergence of the subgroups can be explained by the existence of a large set of cohesive configurations for groups with few individuals, as shown in section 3 and [33]. Crucially, these sets of cohesive configurations are robust to perturbations.

#### 5. Circular configurations

The last set of configurations that we consider are circular configurations. They are commonly observed, for example, in the milling motion of fish schools, where swimmers follow one another, rotating around an empty core [45]. Here, we investigate the role that hydrodynamic interactions play in such configurations. We first consider circular configurations for which the motion is in the same plane as the swimmers, and then configurations for which the primary motion is orthogonal to the plane containing the swimmers.

#### 5.1. In-plane motion

We first consider *N* swimmers that are uniformly distributed along the circumference of a circle of radius *R*. Each swimmer is initially tangent to the circle, as shown in figure 11, which also shows the streamlines of the induced flow.

Since milling behavior is commonly observed in nature, we ask whether it can arise purely from hydrodynamic interactions; that is, are there circular configurations of swimmers that maintain their structure

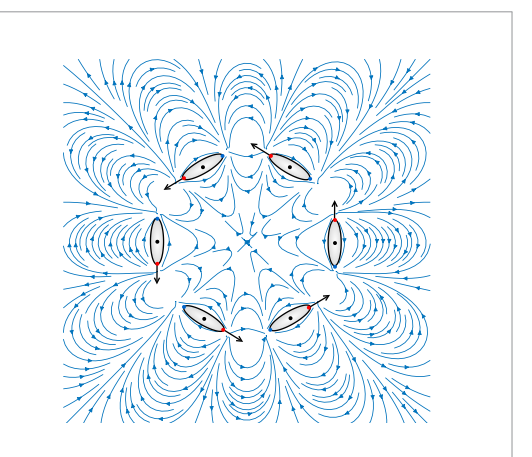


**Figure 11.** Spatial arrangement for swimmers in a circular configuration. Here, N = 6, and the streamlines of the induced flow are also shown.

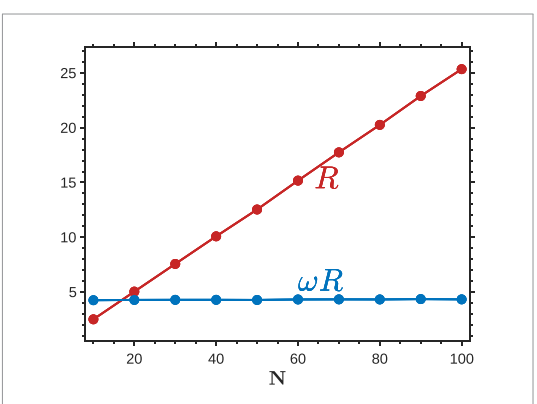


**Figure 12.** The radius R and swimmer speed  $\omega R$  as functions of group size for hydrodynamic milling configurations.

indefinitely? With the aid of a Jacobian-free Newton-Krylov solver (see [46] for details), for every  $N \in$ [4, 100], we find an equilibrium circular configuration in which the swimmers chase each other around the circle. Due to its similarity to milling, and its passive hydrodynamic nature, we refer to this behavior as hydrodynamic milling. The behavior is slightly more complicated than simple rotation around a circle; in addition to rotation around the circle, the swimmers' positions undergo small oscillations on a much faster time scale. Dynamically speaking, the circular configurations give rise to relative periodic orbits. For the sake of simplicity, we may ignore the fast oscillations and approximate the motion as simple rotation around a circle. The radius of the equilibrium circular configuration and the speed at which the swimmers move around the circle are shown as functions of N in figure 12. The radius is a linear function of N, implying that the separation between swimmers remains constant as N increases. The speed of the swimmers is also constant, or, equivalently, the angular rate of rotation of the group,  $\omega$ , is proportional to  $R^{-1}$ .

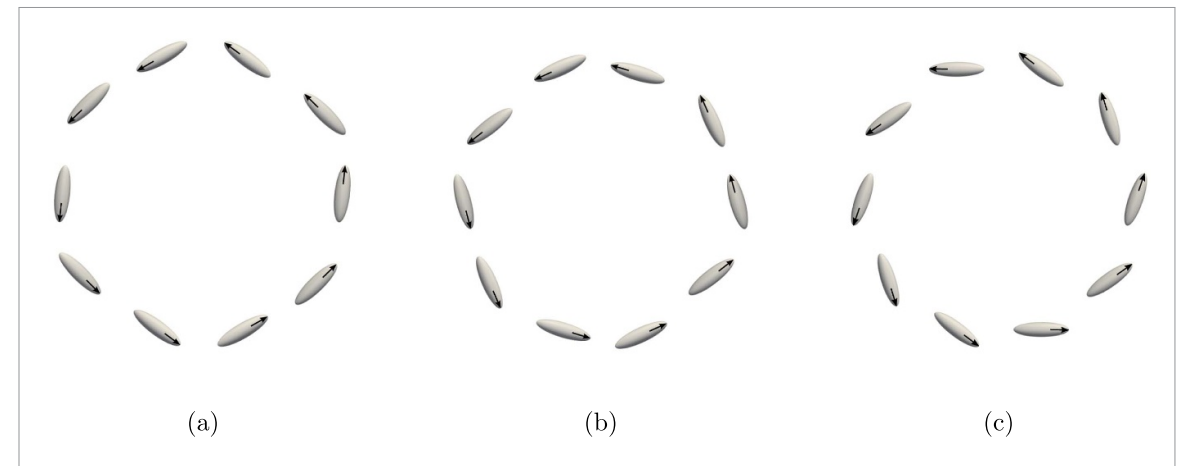


**Figure 13.** Unstable modes of hydrodynamic milling for N = 10. (a) Mode 1 (asymmetric). (b) Mode 2 (conjugate to mode 1). (c) Mode 3 (symmetric).

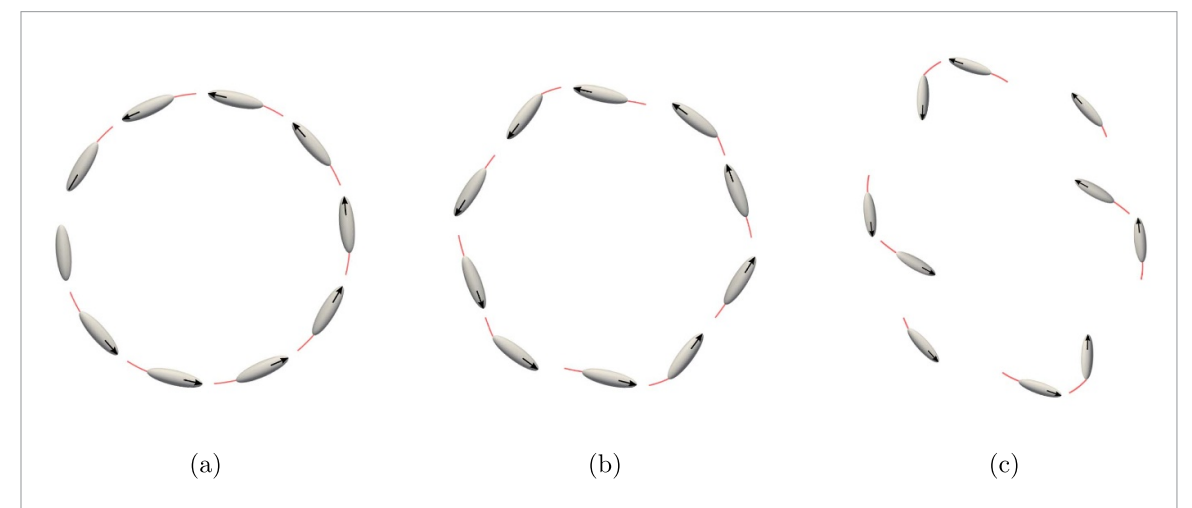


**Figure 14.** Nonlinear evolution of hydrodynamic milling state for N = 10. The red comet tails show the trajectories taken in the near past. (a) Hydrodynamic milling. (b) Onset of instability. (c) Splitting into subgroups.

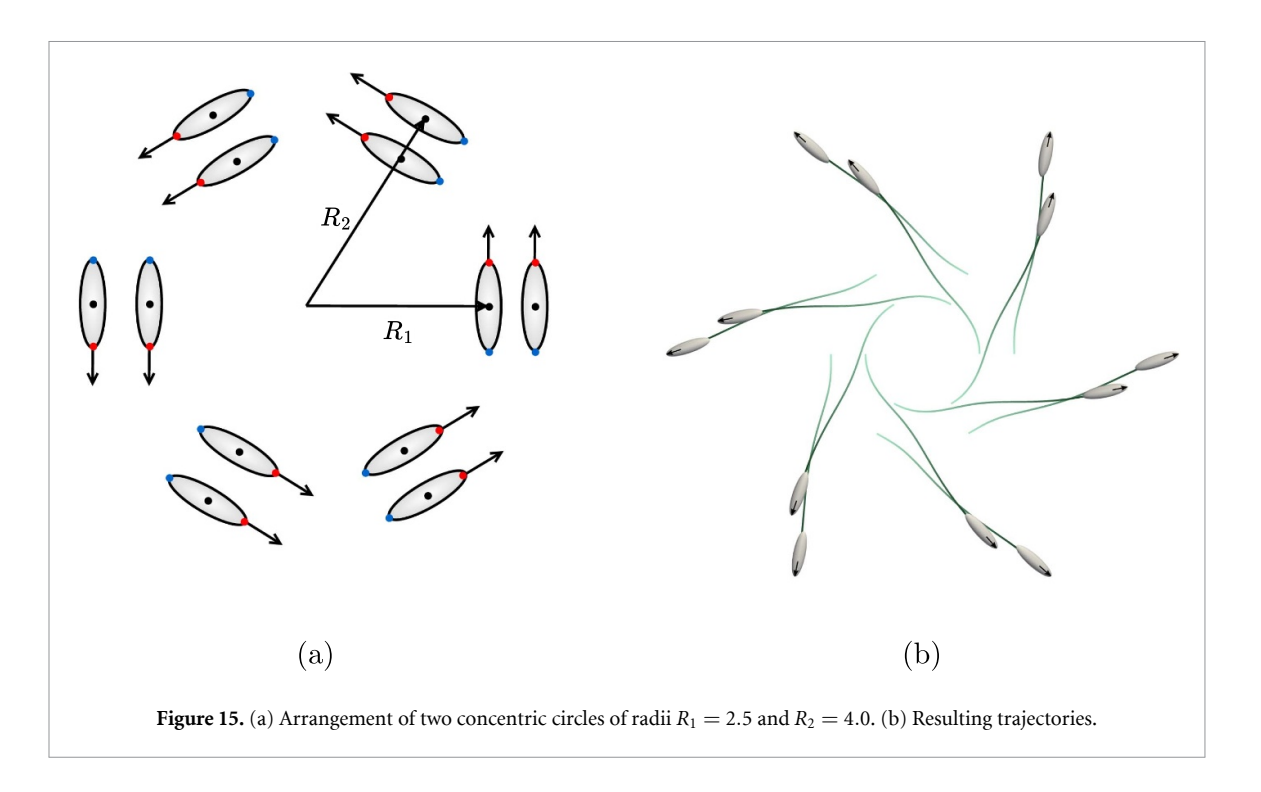
To determine the robustness of hydrodynamic milling, we calculate the linear stability of the associated relative periodic orbits. The technical details are given in the appendix. No matter the size of the group, we find that there are always three unstable modes: two asymmetric modes that form a conjugate pair, and a purely real symmetric mode corresponding to uniform rotation of the swimmers. The unstable modes are shown in figure 13. The conjugate pair always has a faster growth rate than the symmetric mode, which is apparent in the nonlinear simulation shown in figure 14. Beyond the onset of instability, the swimmers split into subgroups before soon colliding.

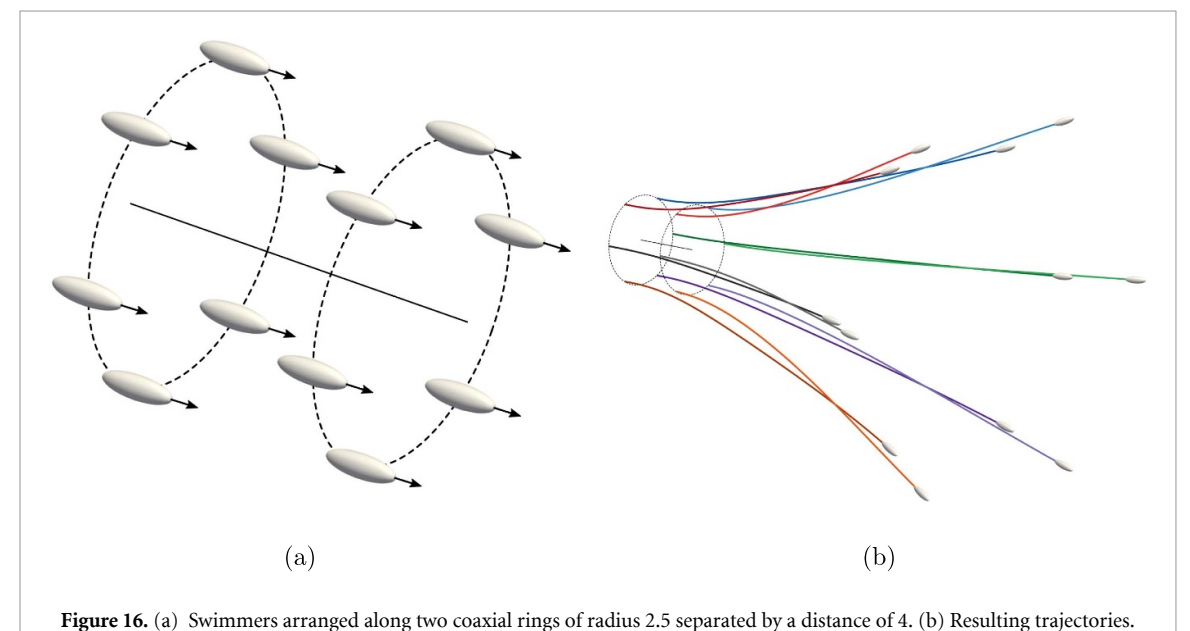
More complex circular arrangements ultimately end with the same fate as the hydrodynamic milling state and the diamond configurations. One such example is shown in figure 15, where twelve swimmers have been initially arranged along two concentric circles. The swimmers destabilize more quickly than in the hydrodynamic milling state, ultimately

splitting into pairs that undergo braided motion, as seen previously. Despite the overall group not being cohesive, the subgroups remain cohesive for all later times.

#### 5.2. Out-of-plane motion

The final configuration we consider again has the swimmers uniformly distributed along the circumferences of two circles (figure 16). The circles are coaxial, of the same size, and are offset from each other along their mutual axis. The swimmers differ now in that their orientations are parallel to the mutual axis of the circles rather than tangent to the circles. As was observed for every other configuration with many swimmers, relatively small subgroups quickly emerge. In this case, swimmers from one circle pair up with their counterparts from the other circle. The pairs undergo braided motions and remain cohesive for the rest of time. Even for this fully three-dimensional configuration and motion, the emergence of small and cohesive subgroups remains a robust phenomenon.





#### 6. Summary and conclusions

In this work, we studied the dynamics and cohesion of freely swimming collectives. Our work was driven by a fundamental question in collective hydrodynamics: can group cohesion be sustained purely through passive hydrodynamic interactions?

To address this question, we developed a reducedorder potential-flow model for the three-dimensional hydrodynamic interactions of freely moving inertial swimmers. The model represents the far-field flow induced by the motion of long, thin swimmers. In isolation, a model swimmer moves along a straight line at a constant speed. In the presence of a group, each swimmer's motion is modified by the flow induced by all other swimmers, leading to highly non-trivial dynamics.

Building on previous work in which pairwise interactions were characterized [33], here we studied groups of  $N \ge 3$  swimmers. We considered three types of configurations that we view as elemental building blocks of arbitrary groups: triangular, diamond, and circular configurations. Under the idealized conditions of our model, we found that far-field interactions alone significantly impact the cohesion of groups of swimmers. This result shows that,

contrary to common belief, interactions with a vortical wake do not solely determine the cohesion of groups of swimmers.

Swimmers in triangular configurations diverge from each other if the aspect ratio of the triangle is too large or too small. For aspect ratios centered about unity, on the other hand, cohesive groups can emerge. When the configuration consists of one leader and two followers, the group is semi-cohesive in the sense that the swimmers are hydrodynamically locked for a finite time before eventually diverging from each other. Flipping the configuration to two leaders and one follower stabilizes the group: a stable equilibrium configuration emerges, one which has a large basin of attraction. The key factor enabling an equilibrium configuration is that the torques the swimmers induce on each other balance, leading to stable rotational dynamics.

For larger groups, cohesion is more difficult to maintain. For diamond configurations, subgroups quickly form at the periphery of the group, and then progressively develop inward into the core. Destabilization occurs first at the periphery because of the asymmetric hydrodynamic interactions experienced by peripheral swimmers, whereas the core is relatively stable due to cancellation of symmetric hydrodynamic interactions. The same principle seems to be at play in higher-fidelity simulations of tethered swimmers, with peripheral swimmers experiencing highly asymmetric pressure distributions that conceivably produce a net torque and lateral force [47]. Eventually, in our simulations, the entire group splits into subgroups that tend to diverge from each other. Despite the loss of cohesion of the overall group, the subgroups that emerge tend to be cohesive and maintain their structure indefinitely. Additionally, our results are suggestive of how the cohesion of the entire group could be maintained. The ultimate loss of cohesion of the group is precipitated by the changing dynamics of the swimmers at the group's edge, while the core is initially stable. The core destabilizes slowly as the destabilization at the edge diffuses inward. We posit that if the swimmers at the edge are actively controlled, then the core of the group will remain stable under passive dynamics.

Similar observations are made for circular configurations of swimmers. Interestingly, we discover the existence of hydrodynamic milling states—circular configurations of swimmers that chase each other around a circle while traveling at constant speed. These states reproduce the milling behavior observed in fish schools, though purely through passive hydrodynamic interactions. From the dynamical point of view, the hydrodynamic milling states are relative periodic orbits, and we find that they are always unstable to three modes of instability. The instabilities cause the group to devolve into smaller subgroups

that are cohesive, similar to the diamond configuration. Qualitatively similar behavior arises for groups built from multiple circular configurations of swimmers: the overall group is not cohesive, but small cohesive subgroups emerge.

Returning to our original question of whether group cohesion can be sustained purely through passive hydrodynamic interactions, our results suggest a negative answer. However, there is hope that cohesion can be maintained without resorting to actively controlling every swimmer in the group. Since cohesive subgroups consistently emerge from larger groups, one would only have to control the interactions between subgroups, rather than between all individuals, to create a larger cohesive group. Furthermore, groups seem to progressively destabilize from their periphery inward. If the edge of the group can be controlled, there is hope that the core will remain passively stable. Such a strategy is successfully employed by shepherds and farmers who use dogs to herd livestock; perhaps a similar strategy is possible in aquatic environments as well.

This work was supported by the University of Houston Grants to Enhance and Advance Research Program, 00 018 9684.

#### Data availability statement

All data that support the findings of this study are included within the article (and any supplementary files).

# Appendix. Linear stability analysis of hydrodynamic milling

Let  $\mathbf{X} \in \mathbb{R}^{6N}$  be the state of the system, as described at the end of section 2. The relative periodic orbits that correspond to hydrodynamic milling are periodic orbits in a frame of reference that rotates with the average rate of rotation of the group. Let  $\mathbf{X}_p(t)$  denote the periodic orbit in the rotating frame of reference, so that  $\mathbf{X}_p(t) = \mathbf{X}_p(t+T)$ , with T the period. One can determine the linear stability of the periodic orbit by performing a Floquet analysis.

Alternatively, one may define a Poincaré section, and a point  ${\bf p}$  along the periodic orbit will be a fixed point of the associated Poincaré map  ${\boldsymbol \phi}$ :  ${\boldsymbol \phi}({\bf p})={\bf p}$ . The linear stability of the periodic orbit is equivalent to the linear stability of  ${\bf p}$  under the discrete dynamics of the Poincaré map. We follow this alternative approach.

To determine the stability of the relative periodic orbit, we require the eigenvalues of the Jacobian of  $\phi$  evaluated at  $\mathbf{p}$ . We estimate the eigenvalues and corresponding eigenvectors using the Arnoldi iteration [48]. The Arnoldi iteration requires the ability to evaluate the product of the Jacobian with any vector.

We may estimate such products by using the Taylor expansion of  $\phi$ , which yields

$$\phi\left(\mathbf{p} + \varepsilon \hat{\mathbf{X}}\right) \approx \phi\left(\mathbf{p}\right) + \varepsilon \nabla \phi\left(\mathbf{p}\right) \hat{\mathbf{X}} \Longrightarrow \nabla \phi\left(\mathbf{p}\right) \hat{\mathbf{X}}$$

$$\approx \frac{\phi\left(\mathbf{p} + \varepsilon \hat{\mathbf{X}}\right) - \phi\left(\mathbf{p}\right)}{\varepsilon}, \quad \varepsilon \ll 1. \quad (A1)$$

Thus, the Jacobian-vector product  $\nabla \phi(\mathbf{p})\hat{\mathbf{X}}$  can be approximated by simply evaluating  $\phi$ . By definition,  $\phi(\mathbf{p}) = \mathbf{p}$ . To get  $\phi(\mathbf{p} + \varepsilon \hat{\mathbf{X}})$ , we perturb  $\mathbf{p}$  on the Poincaré section by  $\varepsilon \hat{\mathbf{X}}$  and use our nonlinear solver to evolve the solver forward in time until the state intersects the Poincaré section.

#### **ORCID** iDs

Mohamed Niged Mabrouk © 0009-0004-6867-8560 Daniel Floryan © 0000-0002-6353-5075

#### References

- [1] Vicsek T and Zafeiris A 2012 Phys. Rep. 517 71
- [2] Parrish J K and Hamner W M 1997 Animal Groups in Three Dimensions: how Species Aggregate (Cambridge University Press) (https://doi.org/10.1017/CBO9780511601156)
- [3] Couzin I D, Krause J, Franks N R and Levin S A 2005 Nature 433 513
- [4] Landeau L and Terborgh J 1986 Animal Behav. 34 1372
- [5] Hemelrijk C K, Reid D A P, Hildenbrandt H and Padding J T 2015 Fish Fish. 16 511
- [6] Major P F 1978 Animal Behav. 26 760
- [7] Colvert B, Chen K and Kanso E 2017 J. Fluid Mech. 818 366
- [8] Pitcher T J, Magurran A E and Winfield I J 1982 Behav. Ecol. Sociobiol. 10 149
- [9] Dorigo M, Theraulaz G and Trianni V 2020 Sci. Robot.5 eabe4385
- [10] Gibouin F, Raufaste C, Bouret Y and Argentina M 2018 Phys. Fluids 30 091901
- [11] Gazzola M, Tchieu A A, Alexeev D, De Brauer A and Koumoutsakos P 2016 J. Fluid Mech. 789 726
- [12] Zhang Y, Ko H, Calicchia M A, Ni R and Lauder G V 2024 PLoS Biol. 22 e3002501
- [13] Ko H, Lauder G and Nagpal R 2023 J. R. Soc. Interface 20 20230357
- [14] Pitcher T J 1986 Functions of shoaling behaviour in teleosts The Behaviour of Teleost Fishes ed T J Pitcher (Springer) pp 294–337
- [15] Weihs D 1973 Nature 241 290
- [16] Ashraf I, Bradshaw H, Ha T-T, Halloy J, Godoy-Diana R and Thiria B 2017 Proc. Natl Acad. Sci. 114 9599

- [17] Zhang Y and Lauder G V 2024 eLife 12 R90352
- [18] Quinn D B, Moored K W, Dewey P A and Smits A J 2014 J. Fluid Mech. 742 152
- [19] Dewey P A, Quinn D B, Boschitsch B M and Smits A J 2014 Phys. Fluids 26 041903
- [20] Daghooghi M and Borazjani I 2015 Bioinsp. Biomim. 10 056018
- [21] Pan Y and Dong H 2020 Phys. Fluids 32 121901
- [22] Pan Y and Dong H 2022 Phys. Fluids 34 111902
- [23] Heydari S, Hang H and Kanso E 2024 eLife 13 R96129
- [24] Vicsek T, Czirók A, Ben-Jacob E, Cohen I and Shochet O 1995 Phys. Rev. Lett. 75 1226
- [25] Couzin I D, Krause J, James R, Ruxton G D and Franks N R 2002 J. Theor. Biol. 218 1
- [26] Calovi D S, Lopez U, Ngo S, Sire C, Chaté H and Theraulaz G 2014 New J. Phys. 16 015026
- [27] Tunstrøm K, Katz Y, Ioannou C C, Huepe C, Lutz M J and Couzin I D 2013 PLoS Comput. Biol. 9 e1002915
- [28] Lafoux B, Moscatelli J, Godoy-Diana R and Thiria B 2023 Commun. Biol. 6 585
- [29] Pavlov D S and Kasumyan A O 2000 J. Ichthyol. 40 S163
- [30] Filella A, Nadal F, Sire C, Kanso E and Eloy C 2018 Phys. Rev. Lett. 120 198101
- [31] Zhou J, Seo J-H and Mittal R 2025 Phys. Fluids 37 011912
- [32] Huang C, Ling F and Kanso E 2024 Proc. Natl Acad. Sci. 121 e2406293121
- [33] Mabrouk M N and Floryan D 2024 *Bioinsp. Biomim.* 20 016014
- [34] Ko H, Girma A, Zhang Y, Pan Y, Lauder G and Nagpal R 2025 Sci. Rep. 15 20249
- [35] Partridge B L 1982 Sci. Am. 246 114
- [36] Tchieu A A, Kanso E and Newton P K 2012 Proc. R. Soc. A Math. Phys. Eng. Sci. 468 3006
- [37] Tsang A C H and Kanso E 2013 J. Nonlinear Sci. 23 971
- [38] Eldredge J D 2019 Mathematical Modeling of Unsteady Inviscid Flows vol 50 (Springer) (https://doi.org/ 10.1007/978-3-030-18319-6)
- [39] Hernandez-Ortiz J P, Stoltz C G and Graham M D 2005 Phys. Rev. Lett. 95 204501
- [40] Hernández-Ortiz J P, de Pablo J J and Graham M D 2007 Phys. Rev. Lett. 98 140602
- [41] Underhill P T, Hernandez-Ortiz J P and Graham M D 2008 Phys. Rev. Lett. 100 248101
- [42] Hernandez-Ortiz J P, Underhill P T and Graham M D 2009 J. Phys.: Condens. Matter 21 204107
- [43] Ryan S D, Haines B M, Berlyand L, Ziebert F and Aranson I S 2011 Phys. Rev. E 83 050904
- [44] Auton T R, Hunt J C R and Prud'Homme M 1988 J. Fluid Mech. 197 241
- [45] Cambui D S, Gusken E, Roehrs M and Iliass T 2018 Physica A 507 289
- [46] Willis A P 2019 arXiv:1908.06730
- [47] Kelly J, Pan Y, Menzer A and Dong H 2023 *Phys. Fluids* 35 041906
- [48] Trefethen L N and Bau D 1997 Numerical Linear Algebra (SIAM) (https://doi.org/10.1137/1.9780898719574)